Ogiso and Tamaribuchi
Earth, Planets and Space (2022) 74:49
https://doi.org/10.1186/s40623-022-01601-w

Earth, Planets and Space

EXPRESS LETTER

Spatiotemporal evolution of tremor activity near the Nankai Trough trench axis inferred from the spatial distribution of seismic amplitudes

Masashi Ogiso* and Koji Tamaribuchi

Abstract

Slow earthquakes have gained importance due to their proximity to the focal regions of megathrust earthquakes. Among slow earthquakes, tectonic tremors have the highest dominant frequency and are thus best resolved. Here, we estimated the locations of tectonic tremors off the Kii Peninsula, southwestern Japan, from December 2020 through January 2021 using the seismograms of the Dense Oceanfloor Network system for Earthquakes and Tsunamis (DONET). The study area is adjacent to the Nankai Trough, where large megathrust earthquakes are known to occur. We successfully estimated the locations of 3578 tectonic tremor events within an area of ~ 130 km in northeast–southwest and ~ 50 km in northwest–southeast directions along the trench axis. Tremor activity differed between the northeastern and southwestern areas of the focal region, which were separated by a central region of markedly low activity. During the study period, tremor activity began at the northeastern edge of the focal region, and expanded to the southwest along the trench axis until reaching the central low-activity region. Renewed tremor activity later began at the southwestern edge of the low-activity region and migrated southwest along the trench axis. We also detected two distinct events similar to rapid tremor reversals that migrated to the northeast, the first of which may have been triggered by the combined effects of teleseismic surface waves and Earth's tides. Such detailed locations of tectonic tremors can be used as a proxy of the stress state in the accretionary prism and/or along the plate boundary in the Nankai Trough.

Keywords: Tectonic tremor, Tremor migration, Seismic amplitude, Nankai Trough

*Correspondence: mogiso@mri-jma.go.jp
Meteorological Research Institute, Japan Meteorological Agency, 1-1 Nagamine, Tsukuba 305-0052, Japan

Graphical Abstract

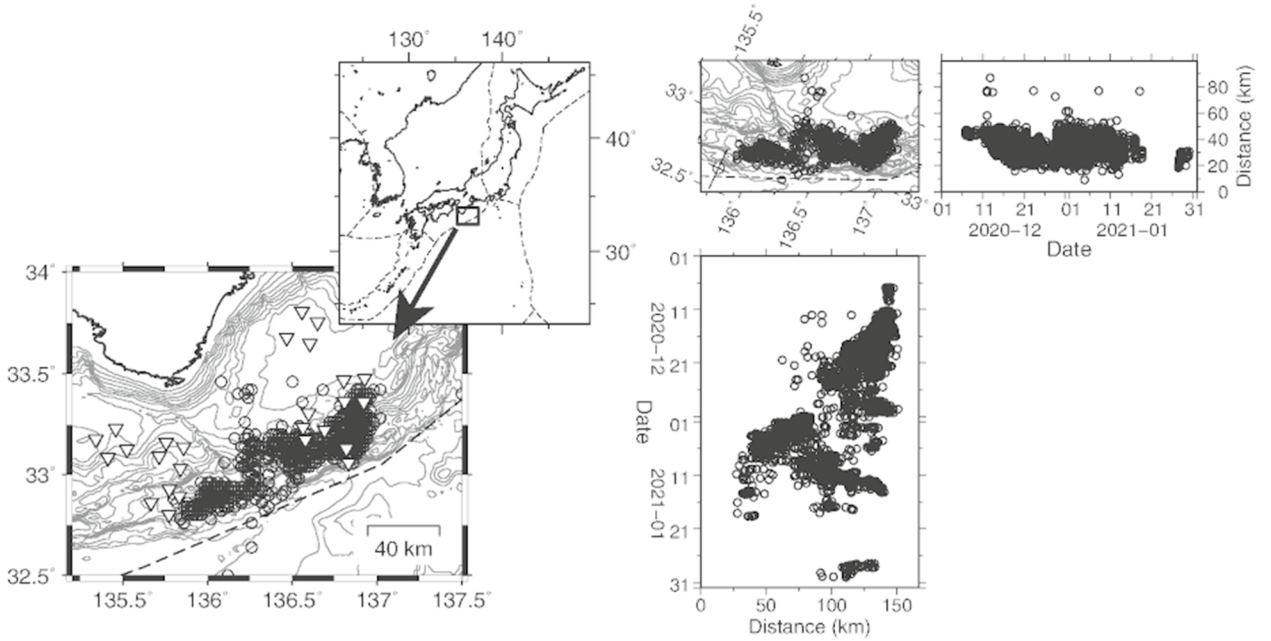

Introduction

Anomalous seismic events called slow earthquakes are governed by a different scaling law than that of typical earthquakes (Ide et al. 2007) and have been observed at plate boundaries around the world (Beroza and Ide 2011). Because the source locations of slow earthquakes tend to be near megathrust earthquakes (Kato et al. 2012; Obara and Kato 2016), the detection of slow earthquakes, as well as regular earthquakes, can provide important information for monitoring the stress state of plate boundaries where devastating earthquakes may occur.

Slow earthquakes are classified into three types based on their characteristic duration and period or frequency: Slow slip events (e.g., Linde et al. 1996; Hirose et al. 1999, 2000) have durations of a few days to years; Very low frequency earthquakes (VLFEs, e.g., Obara and Ito 2005) have dominant periods of a few tens of seconds; and tectonic tremor (e.g., Obara 2002; Kao et al. 2005) has a dominant frequency of a few hertz. Because tectonic tremor lacks the high-frequency energy (> 10 Hz), short-duration tremor events are sometimes called low-frequency earthquakes; indeed, Shelly et al. (2007) interpreted tectonic tremors as swarms of low-frequency earthquakes. These three types of slow earthquakes are sometimes spatiotemporally correlated (e.g., Rogers and Dragert 2003; Obara et al. 2004; Hirose and Obara 2005; Ito et al. 2007; Takeo et al. 2010).

Dense seismic or geodetic networks, which have aided the detection of slow earthquakes, are usually deployed on land [e.g., High sensitivity seismograph network Japan (Okada et al. 2004; Aoi et al. 2020) and the GNSS Earth Observation Network System (Sagiya 2004)]. In contrast, continuous seafloor observations are difficult, and offshore slow earthquakes have been recorded only by temporally installed geophysical equipment (e.g., Obana and Kodaira 2009; Ito et al. 2013; Yamashita et al. 2015; Wallace et al. 2016; Plata-Martinez et al. 2021; Yamashita et al. 2021). The exception is VLFEs, which can be observed using on-land broadband seismometers (Ito and Obara 2006; Asano et al. 2008; Ito et al. 2009). Recently, two dense offshore seismic networks have been deployed around Japan (Aoi et al. 2020): the Dense Oceanfloor Network system for Earthquakes and Tsunamis (DONET) and the Seafloor observation network for earthquakes and tsunamis along the Japan Trench. These networks have been used to reveal detailed tectonic tremor and VLFE activities (Sugioka et al. 2012; To et al. 2015; Toh et al. 2018; Nishikawa et al. 2019; Tanaka et al. 2019; Yamamoto et al. 2022).

In this study, we estimate spatiotemporal locations of tectonic tremor events that occurred off the Kii

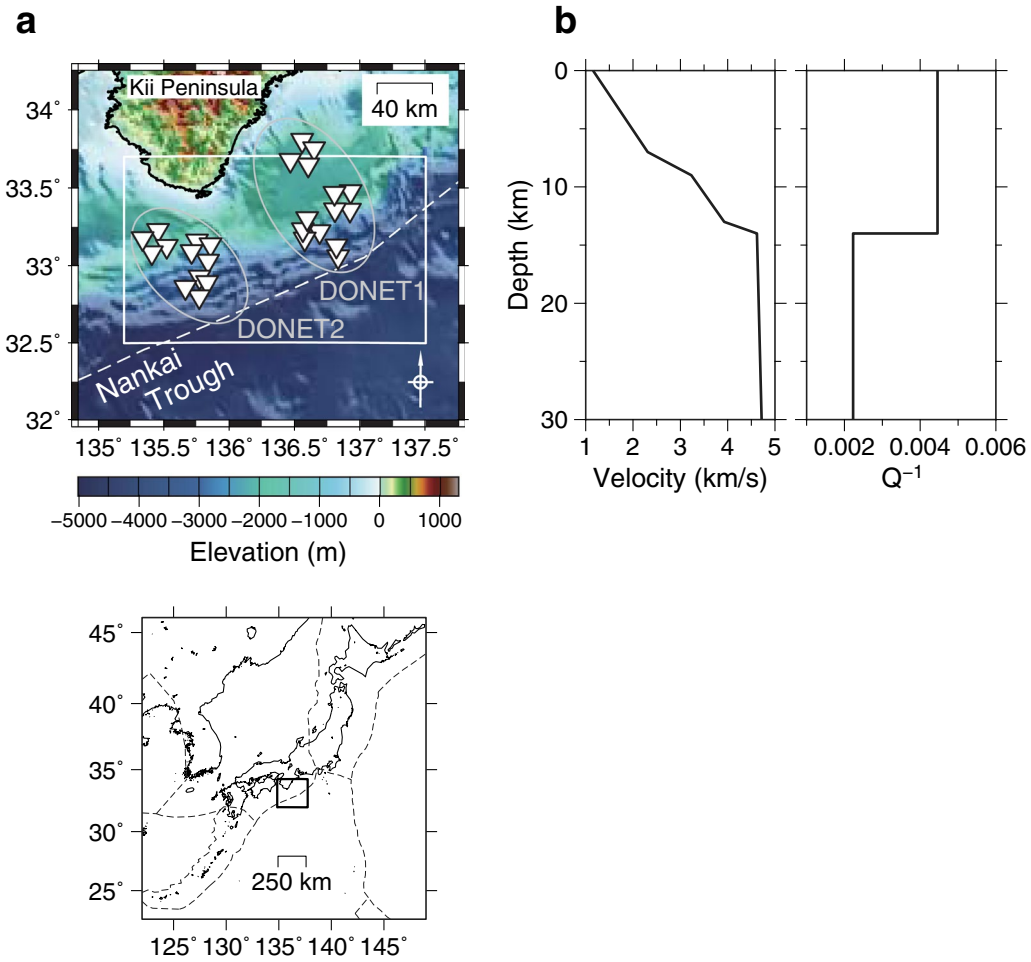

Fig. 1 **a** Regional (bottom) and location (top) maps of the study area and the distribution of DONET seismic stations (white inverted triangles). White rectangle shows the region of our grid search. Topography is from the ETOPO1 model (NOAA National Centers for Environmental Information 2009) and plate boundaries are from Bird (2003). **b** Depth-dependent 1-D S-wave velocity (left) and attenuation (right) structures used in this study

Peninsula (Fig. 1a) from December 2020 through January 2021 using the DONET seismograms. This study area includes part of the Nankai Trough, where several devastating historical earthquakes have occurred (Ando 1975). Since the first detection of tectonic tremors by Obana and Kodaira (2009), characteristics of tremor activity in the area have been investigated from the viewpoint of triggering and migration (Annoura et al. 2017; Tamaribuchi et al. 2019), statistics of the event size distribution (Nakano et al. 2019), and scaling law of seismic energy (Yabe et al. 2019). The other types of slow earthquakes have also been detected, and spatiotemporal correlations among them are one of the important topics in the seismology of slow earthquakes (Obara and Ito 2005; Sugioka et al. 2012; To et al. 2015; Toh et al. 2018; Araki et al. 2017; Takemura et al. 2019a, b; Ariyoshi et al. 2021; Yamamoto et al. 2022). Hence, a detailed analysis of tremor activity using the DONET dense offshore seismic network would contribute to the understanding of the slow earthquake activity in the area.

The envelope correlation method (e.g., Obara 2002; Ide 2010) has been widely used to locate tremors. However, the waveforms of tremors occurring near trench axes have long durations and lack distinct phases because of the heterogeneous seismic structure and the existence of a seawater layer (Takemura et al. 2020). As a result, the correlation coefficient of seismogram envelopes may be low, inducting large uncertainties on differential travel times and widely varying tremor locations. In such cases, locations can alternatively be estimated using seismic amplitudes. Even if the shape of each seismogram envelope shows complicated features, the amplitude decay of a given seismic event can be modeled with geometrical spreading and intrinsic

absorption, because the net loss of seismic energy during wave propagation depends solely on intrinsic absorption. The amplitude source location (ASL) method (Yamasato 1997; Battaglia and Aki 2003; Kumagai et al. 2013, 2019) has been successfully used to estimate locations of long-duration seismic events such as volcanic tremor (Kumagai et al. 2010; Ogiso and Yomogida 2012; Ichihara and Matsumoto 2017; Ichimura et al. 2018; Walsh et al. 2019) and propagation of pyroclastic flows (Jolly et al. 2002), debris flows (Kumagai et al. 2009; Ogiso and Yomogida 2015; Doi and Maeda 2020), and snow avalanches (Pérez-Guillén et al. 2019). Tamaribuchi et al. (2019) applied the ASL method to seismic records recorded by temporary ocean bottom seismometers to reveal spatiotemporal tremor activity in our study area. Therefore, we applied the ASL method to DONET records to reveal tremor activity over a broader region than that analyzed by Tamaribuchi et al. (2019).

All dates and times used in this study are reported in Japan Standard Time (UTC +9 h).

Methods and data

Amplitude source location method

Here, we briefly review the ASL method and its application to locate tremor events (Battaglia et al. 2005; Kumagai et al. 2010). When a seismic source at location i radiates seismic waves of amplitude $A_i^{(s)}(f)$ at frequency f, the seismic amplitude at the jth station, $A_j(f)$, is represented as

$$A_j(f) = A_i^{(s)}(f)\frac{\exp(-\pi f Q_{ij}^{-1}\tau_{ij})}{r_{ij}^n}S_j(f), \tag{1}$$

where τ_{ij} is the travel time, r_{ij} is the hypocentral distance, Q_{ij}^{-1} is the attenuation factor between the ith location and the jth station, and $S_j(f)$ is the site amplification factor at the jth station. The power n depends on the type of propagating waves: $n = 1.0$ for body waves and $n = 0.5$ for surface waves. Equation (1) holds for far-field wave propagation. We assumed that the wave trains of tremors consisted of S-waves, i.e., $n = 1.0$ (see "Data processing", below). If we assume the ith location, we can calculate source radiation amplitude from Eq. (1) as

$$A_i^{(s)}(f) = \frac{1}{N}\sum_{j=1}^{N}\frac{A_j(f)}{S_j(f)}r_{ij}^n \exp(\pi f Q_{ij}^{-1}\tau_{ij}), \tag{2}$$

where N is the number of stations. Then, we define the normalized residual R_i as

$$R_i = \frac{\sum_{j=1}^{N}\{A_j(f)/S_j(f) - A_i^{(s)}(f)\exp(-\pi f Q_{ij}^{-1}\tau_{ij})/r_{ij}^n\}^2}{\sum_{j=1}^{N}\{A_j(f)/S_j(f)\}^2}, \tag{3}$$

and conduct a grid search for the location that minimized R_i. We performed our grid search between 135.7° and 137.5° E and between 32.5° and 33.7° N in increments of 0.02°, and from 0 and 20 km depth in increments of 2 km (Fig. 1a).

Data set

We used a subset of the DONET ocean-bottom seismometers operated by the National Research Institute for Earth Science and Disaster Resilience (NIED, National Research Institute for Earth Science and Disaster Resilience 2019; Aoi et al. 2020). DONET comprises of two subnetworks: DONET1 (22 stations) and DONET2 (29 stations). Each DONET station has two seismometers: a strong motion accelerometer and a broadband velocity seismometer. We selected 14 and 12 stations from DONET1 and DONET2, respectively (Fig. 1a; Additional file 1: Table S1), and then collected the continuous waveforms recorded by the broadband sensor at each station from 1 December 2020 through 31 January 2021.

Figure 1b shows the 1-D S-wave velocity and attenuation structures used herein. Nakanishi et al. (2002) estimated 2-D P-wave velocity structures along several seismic profiles perpendicular to the trench axis of the Nankai Trough. We chose P-wave velocities near the trench axis in the study area from Nakanishi et al. (2002, their Figure 10), and then constructed the 1-D S-wave velocity structure by assuming a Poisson solid. The accretionary prism corresponds to the depth of shallower than 7 km and the subducting Philippine Sea plate to 7–14 km depth. We approximated the distance-dependent attenuation strength of Yabe et al. (2021) as being homogeneous (0.02 km^{-1}) and converted it to Q^{-1} by multiplying $\pi f/\beta$, where $\beta = 3.5$ km/s. Depths > 14 km corresponds to the upper mantle, so we set the value of Q^{-1} in the upper mantle to be half that in the upper layer.

Data processing

We applied a bandpass filter with a frequency range of 2–8 Hz to the vertical component of each seismogram, which is the dominant frequency of tectonic tremors (Obana and Kodaira 2009; Tamaribuchi et al. 2019). The frequency f in Eq. (1) was set to 5.0 Hz, and the site amplification factor $S_i(f)$ at each station was taken as that estimated by Yabe et al. (2021). Because surface waves at this frequency range should be attenuated rapidly, we assumed that the tremor waveforms in this frequency range were composed of S-waves and set $n = 1.0$ in Eqs. (1–3). We calculated the root mean square (RMS) amplitude at the jth station, $A_{ij}(f, t_0)$, in 60-s time windows from the bandpass filtered seismogram, which we took as the observed amplitude of tremor at an arbitrary location i and origin time t_0:

$$A_{ij}(f,t_0) = \left\{ \frac{1}{M} \sum_{k=0}^{M-1} v_j^2(f, t_0 + \tau_{ij} + k\Delta t) \right\}^{1/2}, \quad (4)$$

where $v_j(f,t)$ is the vertical component of bandpass-filtered seismograms at the jth station, Δt is the sampling interval of seismograms at the jth station, and M is the number of data used to calculate the RMS amplitude. The sampling interval at each DONET station was 0.01 s, so $M = 6000$ in this study. We checked the quality of $A_{ij}(f,t_0)$, i.e., whether it could be used in the ASL method, based on two aspects: the signal-to-noise ratio and the amplitude ratio among several frequency ranges at each station (Sit et al. 2012; Katakami et al. 2017). First, we defined the amplitude of noise at each station to be the RMS amplitude calculated from $v_j(f,t)$ during the 60-s time window beginning at 01:00 on 1 December 2020, because no tremors and regular earthquakes occurred, and the amplitude of ambient noise was low in this period. We calculated the ratio between $A_{ij}(f,t_0)$ and the noise amplitude at each station and rejected data for which the ratio was lower than 3.0. Next, we checked the amplitude ratio of different frequency ranges at each station. We applied bandpass filters to the three frequency ranges $f_1 = 0.02-0.1$ Hz, $f_2 = 2.0-5.0$ Hz, and $f_3 = 10.0-15.0$ Hz in the vertical components of seismograms from each station, producing three seismograms denoted $v_j(f_1,t)$, $v_j(f_2,t)$, and $v_j(f_3,t)$. Then, we calculated the RMS amplitude in these frequency ranges for each assumed grid of tremor locations and origin time following Eq. (4) and calculated the ratio of these RMS amplitudes $R_{ij}^{\mathrm{FS}}(t_0)$ as

$$R_{ij}^{\mathrm{FS}}(t_0) = \frac{A_{ij}^2(f_2,t_0)}{A_{ij}(f_1,t_0)A_{ij}(f_3,t_0)}, \quad (5)$$

where $A_{ij}(f_1,t_0)$, $A_{ij}(f_2,t_0)$, and $A_{ij}(f_3,t_0)$ are the RMS amplitudes in the frequency ranges f_1, f_2, and f_3, respectively, calculated in a 60-s time window at the jth station. $A_{ij}(f_1,t_0)$, $A_{ij}(f_2,t_0)$, and $A_{ij}(f_3,t_0)$ correspond to the indices of teleseismic surface waves, tectonic tremors, and regular earthquakes, respectively (Sit et al. 2012). Although we used the RMS amplitudes in the frequency range of 2–8 Hz for the estimation of tremor locations, we excluded the frequency range of 5–8 Hz for f_2, as Sit et al. (2012) did, because regular earthquakes also had significant seismic energy at a frequency higher than 5 Hz (Obana and Kodaira 2009; Tamaribuchi et al. 2019). Large $R_{ij}^{\mathrm{FS}}(t_0)$ value indicates that $A_{ij}(f_2,t_0)$ is dominant; therefore, tremor wavetrains that excited at the origin time t_0 at the ith location should arrive at the jth station. We discarded $A_{ij}(f,t_0)$ if $R_{ij}^{\mathrm{FS}}(t_0)$ was lower than 5.0.

After these two quality checks, we counted the number of available $A_{ij}(f,t_0)$ values for each grid of tremor locations, adding new criteria that (1) the hypocentral distance between the ith grid and the jth station should be shorter than 100 km and (2) the station at the shortest hypocentral distance must pass the quality checks. When between 6 and 20 $A_{ij}(f,t_0)$ values were available in the ith grid, we calculated R_i in the grid following Eq. (3). The lower limit of available $A_{ij}(f,t_0)$ was set to 6 to guarantee the precision of determined tremor locations, whereas the upper limit was set to 20 to exclude non-tectonic-tremor seismic events such as teleseismic earthquakes, which are observed at many stations. Finally, we searched for the location with the smallest value of R_i among all grids at the assumed origin time t_0.

We defined the confidence interval on the location of each tremor to be the range, where the logarithm of residual was less than twice its minimum value, because the logarithm of residual varied smoothly, as with a normal distribution. Additional file 1: Figures S1 and S2 show the spatial distributions of residuals and latitudinal, longitudinal, and depth confidence intervals for two example events. The station geometry controls the range of confidence intervals (e.g., Walsh et al. 2017). If a tremor event occurred in a location surrounded by many stations, as in Additional file 1: Fig. S1, both the latitudinal and longitudinal confidence intervals were small (< 0.08° in the case of Additional file 1: Fig. S1), whereas the confidence intervals were large for tremor events that occurred between the DONET1 and DONET2 subnetworks (< 0.22° in the case of Additional file 1: Fig. S2). Constraining the depths of tremor events is more difficult; we were only able to constrain the events in Additional file 1: Figs. S1 and S2 to 4–14 and 4–20 km depth, respectively. All stations locate above tremors and the variation of ray incident angles is smaller than that of azimuthal angles for a certain tremor; therefore, the confidence intervals of depths become larger than those of horizontal locations.

Screening tremor locations

We conducted a grid search every 10 s beginning at 00:00 on 1 December 2020 and ending at 23:59 on 31 January 2021. As a result, we derived a time series of source radiation amplitude $A_i^{(\mathrm{s})}(f,t_0)$ and tremor locations. Because each tremor might have lasted for several tens of seconds, whereas we estimated tremor locations every 10 s, we might have derived several locations for the same tremor event. Therefore, we screened for duplicate tremor locations by checking the temporal variations of tremor locations and source radiation amplitudes of three successive origin times. We used two criteria to select the

appropriate tremor location for further analyses. First, the source radiation amplitude must have been a local maximum. This criterion guarantees that the 60-s time window at each station captured the largest amplitude part of the corresponding tremor signal. If a time window contained the main part of a tremor signal, $A_{ij}(f, t_0)$ and consequently $A_i^{(s)}(f, t_0)$ became larger than those for assumed origin times 10 s earlier and later. Second, we checked whether the difference between the epicenter of a given tremor and those determined for assumed origin times 10 s earlier and later was less than 0.06° (i.e., three grids), both longitudinally and latitudinally. This criterion evaluates the temporal stability of tremor epicenters. Because tremors have long durations, the epicenter of a given tremor should not vary within three successive assumed origin times. Furthermore, if we had picked a tremor location for an assumed origin time 20 s earlier, we compared their residuals and disregarded the events with larger residuals. Figure 2 shows the observed waveform at station KMB08 and the source radiation amplitude time series from 09:00 to 09:40 on 13 December 2020. Several tremor events are recognizable in Fig. 2a, and the source radiation amplitude increases as the observed amplitude increases, implying the occurrence of tremor. The short-duration "pulses" in the time series of source radiation amplitude occur when a time window at each station captures a part of a tremor event. In those cases, $A_{ij}(f, t_0)$ may show little difference among stations, which, together with the large source radiation amplitude, inducting that the tremor locations are determined far from the station array. Such tremor locations strongly depend on the assumed origin time, and we successfully disregard them by comparing locations determined during three successive assumed origin times.

After the screening, we eliminated any tremor locations that corresponded to regular earthquakes. Referring to the Japan Meteorological Agency's unified earthquake catalog, we calculated the theoretical arrival times at 33.0° N, 136.5° E and 0 km depth (i.e., the center of the determined tremor focal region) of P- and S-waves originating from regular earthquakes. If either the P- or S-wave arrival time was within the 60-s time window after the origin time of an arbitrary tremor location, we disregard that location, because $A_{ij}(f, t_0)$ might have originated from the regular earthquake instead of a tremor event. Finally, we visually checked the observed waveforms of all stations and eliminated 45 locations corresponding to wave trains from non-tremor events such as teleseismic earthquakes.

Results and discussion

We successfully estimated 3578 tremor locations; the hypocentral distribution of these tremor events are shown in Fig. 3. Most events are within the area of 130 km in northeast–southwest and 50 km in northwest–southeast directions along the trench axis. About 80% of the tremor events occurred closer to the DONET1 network, and 95% of the events were shallower than 14 km depth. The focal region of tremors in this study extends further southwest than that of Annoura et al. (2017) and Tamaribuchi et al. (2019). Overall, the focal region of all tremor events does not coincide with areas of peak shear stress accumulation rate on the plate boundary as estimated by Noda et al. (2018), consistent with VLFE locations (Takemura et al. 2019b).

Figure 4 shows temporal variations of tremor locations parallel and normal to the trench axis. One obvious feature of the tremor locations is a region of low activity around 32.8° N and 136.5° E. Although this low-activity region is obvious in this study, it is unclear whether it is common to all tremor events occurring in this area or specific of this analysis period; further investigation requires estimating tremor locations for a longer period than in this study. When focusing on temporal variations parallel to the trench axis, tremor activities differ to the northeast and southwest of the low-activity region. Tremor activity during the study period began at the northeastern edge of the focal region on 6 December. Then, the focal region expanded southwest along the trench axis with a velocity of 3–4 km/day. The expansion stopped when the expansion front reached the low-activity region around 24 December. We note that this expansion of the focal region is distinct from the well-known migration of tremor locations reported in many previous studies (e.g., Yamashita et al. 2015; Annoura et al. 2017; Kurihara et al. 2018; Tamaribuchi et al. 2019; Kato and Nakagawa 2020). On 30 December, renewed tremor activity began at the southwestern edge of the low-activity region; This activity migrated (not expanded) to the southwest at 8 km/day until 6 January, roughly twice the earlier expansion velocity northeast of the low-activity region. On 28 December and 11 January, the above activity was accompanied by intensive tremor migrations to the northeast, in both cases at velocities of 10 km/day. These two events resembled rapid tremor reversals (RTRs), but the migration velocities were much slower than those reported by Houston et al. (2011) and Sagae et al. (2021). We speculate the difference between migration velocities of our results and those of previous studies

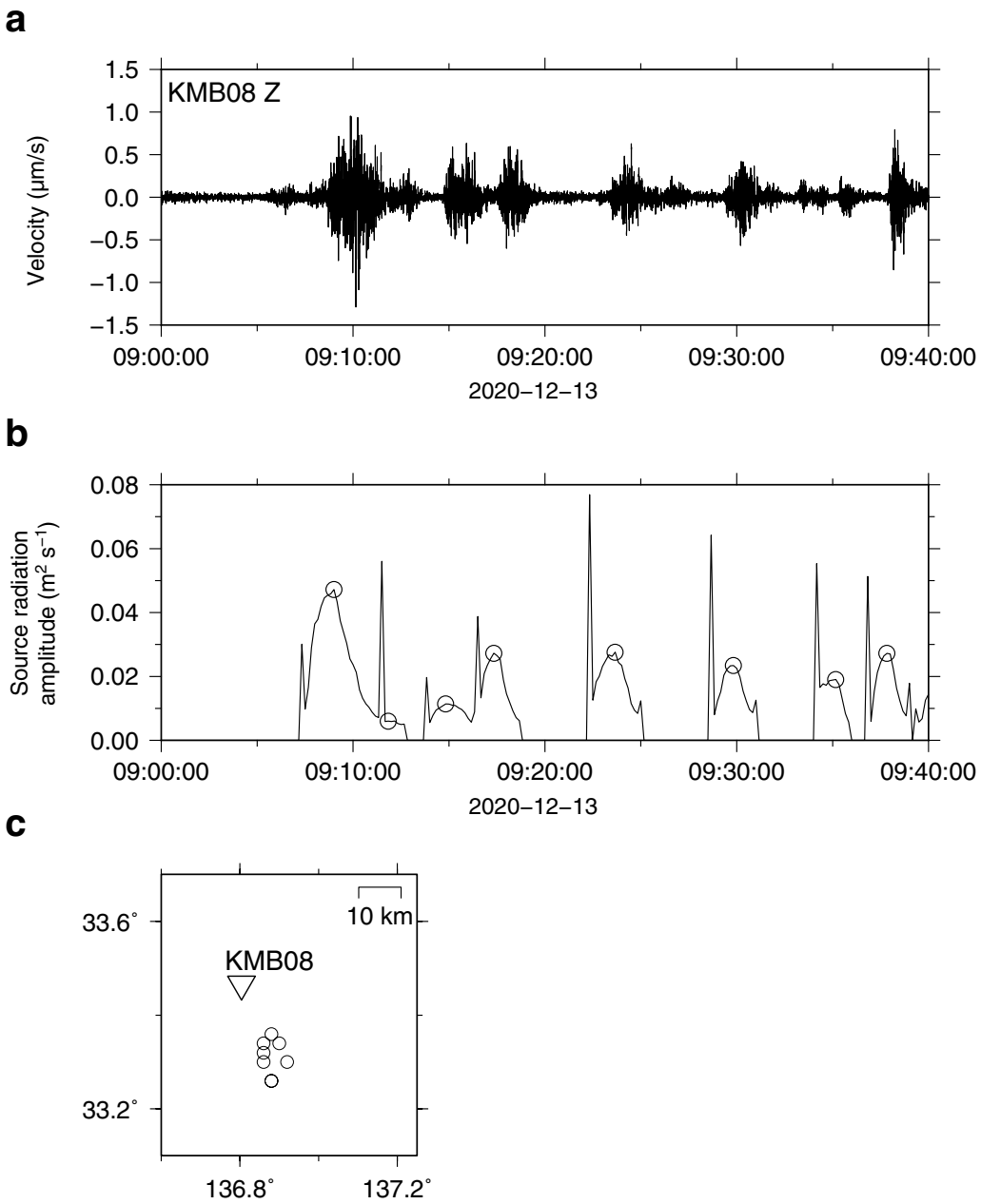

Fig. 2 **a** 2–8 Hz bandpass-filtered vertical-component waveform at station KMB08 and **b** temporal variation of source radiation amplitude between 09:00 and 09:40 on 13 December 2020. Circles denote the origin times of selected tremor locations after screening. **c** Locations of station KMB08 and the tremor events selected in **a** and **b**

to the difference of the tectonic settings. The depths of tremor locations in this study are shallower than those of Houston et al. (2011) and Sagae et al. (2021) so that the generation environment of tremors should also differ. Quantitative discussion of migration velocities is future work.

The historical seismicity along the Nankai Trough described by Ando (1975) implies that the distinct peaks in the stress accumulation rate estimated by Noda et al. (2018) correspond to the asperities of large earthquakes. The focal region of tremors estimated herein is located

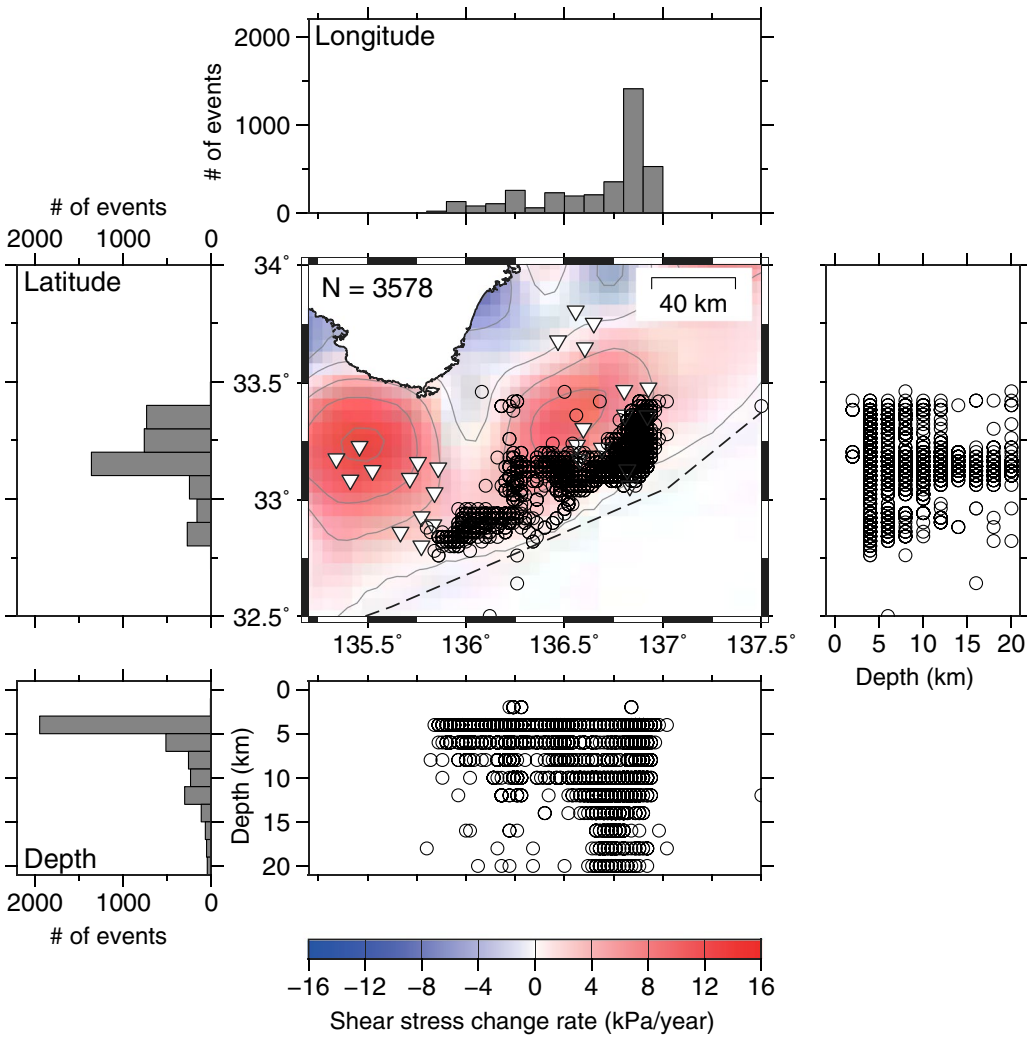

Fig. 3 Epicenters, vertical cross sections and the histograms of longitudinal, latitudinal, and depth distributions of tremor locations determined herein between 1 December 2020 and 31 January 2021. Circles are tremor locations, and inverted triangles are DONET stations. The longitudinal and latitudinal histograms have bin sizes of 0.1°, and the depth histogram has bin size of 2 km. Color contours describes the shear stress accumulation rate at the plate boundary estimated by Noda et al. (2018)

within the shallower extent of these asperities. Whether the focal region of tremors ruptures during a megathrust earthquake should be a key control on the nucleation of a tsunamigenic earthquake. Park et al. (2014) reported a periodical variation of reflection coefficients, which correlate with the amount of fluids, on the décollement along the Nankai Trough (Fig. 4). The northeastern side of the whole focal region of tremors in this study coincides with the region of positive reflection coefficients while southwestern the negative reflection coefficients. Park et al. (2014) interpreted the regions of positive reflection coefficients as conditionally stable patches while negative as unstable seismogenic patches, based on the relationship between an amount of fluids and elastic strain accumulation. Spatial correlation between the distribution of reflection coefficients and the tremor activity in our study area implies that the spatial variation of tremor activity would be an indirect measurement of strain (and stress) distribution, and temporal change of tremor activity might be a proxy of the strain (and stress) state there. An advantage of monitoring tremor activity is the number of events. In general, tremor events outnumber VLFEs (e.g., Tamaribuchi et al. 2019), so it may be possible to derive more detailed spatiotemporal features from tremors than from VLFEs.

The difference between tremor activities to the northeast and southwest of the low-activity region is also evident in the time series of source radiation amplitudes

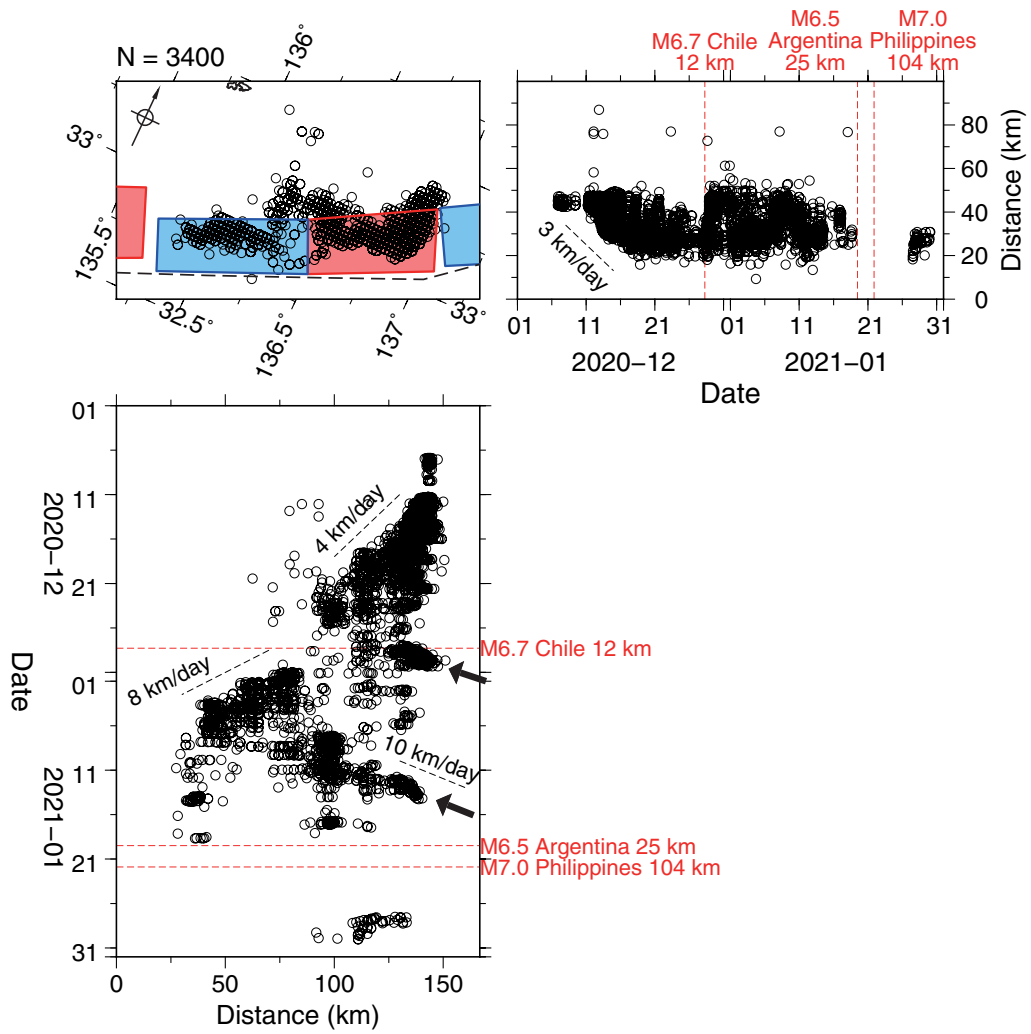

Fig. 4 Temporal variation of tremor locations along and normal to the trench axis. We selected tremors at depths shallower than 14 km and rotated map view N30° E that is parallel to the strike of the trench axis. The origin of the distances is (32.45° N, 135.7° E). Red and blue polygons in the map view indicate the areas of positive and negative reflection coefficients on the décollement, respectively. We visually determined the locations of these areas from Fig. 1 of Park et al. (2014). The thick black dashed line in the map view indicates the trench axis. Red dashed lines denote the origin time of teleseismic earthquakes, for which the approximate location, depth, and magnitude estimated by the GCMT project (Ekström et al. 2012) are reported. Black arrows indicate two RTR-like activities (see "Results and discussion")

(Fig. 5a). Tremor events with large source radiation amplitudes ($\geq 0.05\ m^2/s$) mainly occurred in December, i.e., to the northeast of the low-activity region. In contrast, the source radiation amplitudes of tremor events to the southwest tended to be small, as were those of tremor events that occurred to the northeast in January. We note that the source radiation amplitude is affected by both the maximum amplitude and duration of the source time function; our use of a fixed 60-s time window in calculating observed amplitudes would result in the radiated

(See figure on next page.)

Fig. 5 **a** Temporal variation of source radiation amplitude (circles) compared to the cumulative number of tremor events (solid curve). **b** ΔCFF at the plate boundary in our study area due to Earth's tides. **c** Hourly number of tremor events (bars) and ΔCFF (dashed curve) during 27–30 December 2020. Red dashed lines denote the origin time of teleseismic earthquakes, for which the approximate location, depth, and magnitude estimated by the GCMT project (Ekström et al. 2012) are reported

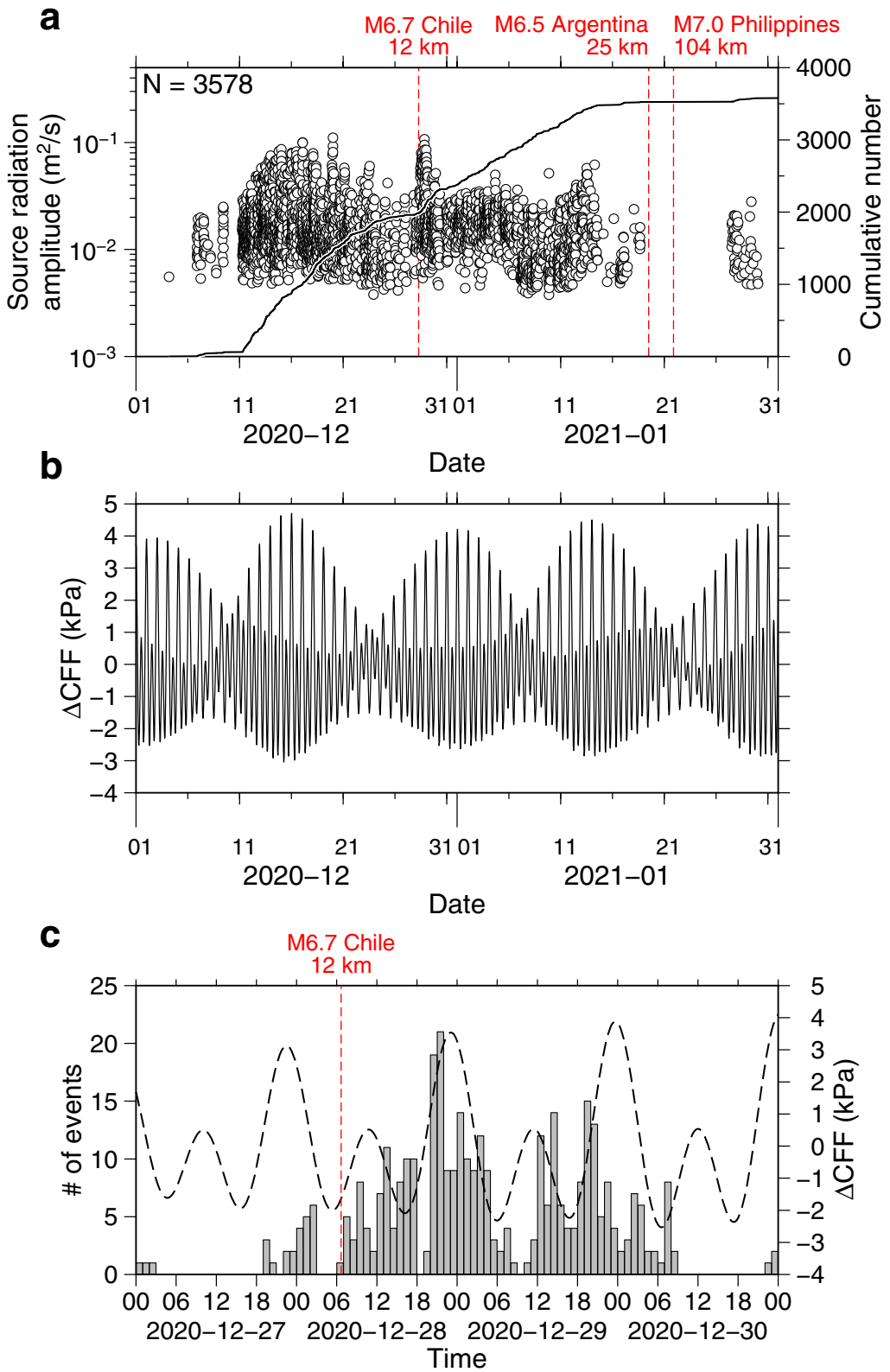

Fig. 5 (See legend on previous page.)

seismic energy being underestimated if the duration of the tremor event was less than 60 s. Quantitative analysis of the observed spatiotemporal variation of source radiation amplitudes is beyond the scope of this study.

External disturbances such as the propagation of seismic waves from regional or teleseismic earthquakes or the Earth's tides are known to trigger tremor events (Nakata et al. 2008; Ide 2010; To et al. 2015; Annoura et al. 2017; Tamaribuchi et al. 2019). Here, we compared the observed tremor activity with the global seismicity and Earth's tides. Figure 5b shows the variation of Coulomb's failure function (ΔCFF) at the plate boundary around the focal region of the observed tremors. We calculated ΔCFF following the procedure of Hirose et al. (2019) with the following fault parameters: strike 258°, dip 7°, and rake 123°. The predominant ΔCFF variations are semidiurnal and semimonthly, whereas the cumulative number of tremor events increased at an almost constant rate from 11 December until 18 January (Fig. 5a). Therefore, we conclude that the semimonthly tidal period had little influence on the occurrence of tremor during the study period.

According to the Global Centroid–Moment–Tensor (GCMT) catalog (Ekström et al. 2012), three teleseismic earthquakes with magnitudes larger than 6.5 occurred during the analysis period (Figs. 4 and 5a). The M6.7 earthquake near Chile preceded RTR-like activity in late December. In contrast, the M6.5 earthquake near Argentina was followed by a pause in tremor activity, and the M7.0 earthquake at intermediate depth near the Philippines occurred during a pause in activity, and thus seems to have had no influence on tremor activity. Although it seems that the M6.5 Argentina earthquake might have caused the tremor activity to cease, demonstrating such a causal relationship between seismic waves and the prevention of tremor events is difficult and will be the subject of future work.

Figure 5c directly compares the number of tremor events per hour to the ΔCFF due to the Earth's tides before and after the M6.7 Chile earthquake. Increased tremor activity persisted for about 48 h after the earthquake, during which time and the hourly number of tremors gradually increased for the first 12 h and then gradually decreased during the following 36 h. During the same period, the hourly number of tremors seems to correlate with the semidiurnal variations of Δ CFF. In contrast to the semimonthly tidal period, the twice-daily energy of the Earth's tides seems to have affected the occurrence of tremors during the transient RTR-like activity during 28–30 December. Considering the lag time between the arrival of large-amplitude surface waves (about 50 min after the origin time) and the increase in the number of tremor events, the RTR-like activity during 28–30 December may have been caused by the combined effects of stress disturbances by the teleseismic surface waves and Earth's tides rather than the dynamic triggering only by surface waves.

Conclusions

We estimated the detailed location of tectonic tremor events off the Kii Peninsula, southwest Japan, from December 2020 through January 2021 using the ASL method. The tremors were distributed in a focal region of roughly 130 km in northeast–southwest and 50 km in northwest–southeast directions along the trench axis. The main period of tremor activity was between 11 December and 18 January. We found a region of markedly low activity region at the center of the focal region. Most tremor events (80%) occurred in the northeastern part of the focal region. Tremor activity began at the northeastern edge of the focal region and expanded to the southwest at a velocity of 3–4 km/day until the expansion front reached the central low-activity region. At the end of December, renewed tremor activity began from the southwestern edge of the low-activity region and tremor locations migrated southwest at a velocity of ∼8 km/day. We also detected two RTR-like tremor events during the study period, the earlier of which possibly triggered by the combined effects of teleseismic surface waves and Earth's tides. The locations of tectonic tremors estimated by the ASL method may prove useful for analyzing spatiotemporal features of tremor, such as the triggering tremor events by external disturbances and stress state in the focal region of tremors.

Abbreviations

ASL: Amplitude source location; CFF: Coulomb's failure function; DONET: Dense Oceanfloor Network system for Earthquakes and Tsunamis; GCMT: Global Centroid–Moment–Tensor; NIED: National Research Institute for Earth Science and Disaster Resilience; RMS: Root mean square; RTR: Rapid tremor reversal; VLFE: Very low frequency earthquake.

Supplementary Information

The online version contains supplementary material available at https://doi.org/10.1186/s40623-022-01601-w.

Additional file 1. Supplementary table and figures. **Table S1.** Locations and site amplification factors of stations used in this study. **Figure S1.** Residual distribution for the tremor event that occurred at 09:09:00 on 13 December 2020. **Figure S2.** Residual distribution for the tremor event that occurred at 01:08:30 on January 2021.

Acknowledgements

We thank the NIED staff for maintaining and providing the DONET seismic records. We also thank Suguru Yabe for providing the site amplification factors of DONET stations (Yabe et al. 2021), Akemi Noda for providing the digital data on the shear stress accumulation rate at the plate boundary along the Nankai Trough (Noda et al. 2018), and Fuyuki Hirose for providing the software to calculate ΔCFF (Hirose et al. 2019). We referred to the ETOPO1 Global Relief

Model (NOAA National Centers for Environmental Information 2009) for drawing maps and calculating tremor locations, and the plate boundary model compiled by Bird (2003) to plot plate boundaries in the figures. All figures were drawn using Generic Mapping Tools (Wessel et al. 2013). Comments from two anonymous reviewers improved the manuscript.

Authors' contributions
MO estimated tremor locations and drafted the manuscript. KT proposed the methods for quality checking the observed waveforms and screening the tremor locations, and investigated the influence of Earth's tides on tremor activity. Both authors read and approved the final manuscript.

Funding
Not applicable.

Availability of data and materials
The DONET waveforms (National Research Institute for Earth Science and Disaster Resilience 2019) can be downloaded from the NIED webpage (https://www.hinet.bosai.go.jp/?LANG=en). The unified earthquake catalog can be downloaded from the the Japan Meteorological Agency's webpage (https://www.data.jma.go.jp/svd/eqev/data/bulletin/index_e.html) as well as the NIED webpage (https://www.hinet.bosai.go.jp/?LANG=en). The GCMT catalog can be downloaded from the project's webpage (https://www.globalcmt.org). The source codes used in this study can be downloaded from https://github.com/mogiso/AmplitudeSourceLocation.

Declarations

Ethics approval and consent to participate
Not applicable.

Consent for publication
Not applicable.

Competing interests
The authors declare that they have no competing interests.

Received: 27 December 2021 Accepted: 4 March 2022
Published online: 29 March 2022

References

Ando M (1975) Source mechanisms and tectonic significance of historical earthquakes along the Nankai Trough, Japan. Tectonophysics 27(2):119–140. https://doi.org/10.1016/0040-1951(75)90102-X

Annoura S, Hashimoto T, Kamaya N, Katsumata A (2017) Shallow episodic tremor near the Nankai Trough axis off southeast Mie prefecture, Japan. Geophys Res Lett 44(8):3564–3571. https://doi.org/10.1002/2017GL073006

Aoi S, Asano Y, Kunugi T, Kimura T, Uehira K, Takahashi N, Ueda H, Shiomi K, Matsumoto T, Fujiwara H (2020) MOWLAS: NIED observation network for earthquake, tsunami and volcano. Earth Planets Space 72(1):1–31. https://doi.org/10.1186/s40623-020-01250-x

Araki E, Saffer DM, Kopf AJ, Wallace LM, Kimura T, Machida Y, Ide S, Davis E (2017) Recurring and triggered slow-slip events near the trench at the Nankai Trough subduction megathrust. Science 356(6343):1157–1160. https://doi.org/10.1126/science.aan3120

Ariyoshi K, Iinuma T, Nakano M, Kimura T, Araki E, Machida Y, Sueki K, Yada S, Nishiyama T, Suzuki K, Hori T, Takahashi N, Kodaira S (2021) Characteristics of slow slip event in March 2020 revealed from borehole and DONET observatories. Front Earth Sci 8:22. https://doi.org/10.3389/feart.2020.600793

Asano Y, Obara K, Ito Y (2008) Spatiotemporal distribution of very-low frequency earthquakes in Tokachi-oki near the junction of the Kuril and Japan trenches revealed by using array signal processing. Earth Planets Space 60(8):871–875. https://doi.org/10.1186/BF03352839

Battaglia J, Aki K (2003) Location of seismic events and eruptive fissures on the Piton de la Fournaise Volcano using seismic amplitudes. J Geophys Res 108(B8):2364. https://doi.org/10.1029/2002JB002193

Battaglia J, Aki K, Ferrazzini V (2005) Location of tremor sources and estimation of lava output using tremor source amplitude on the Piton de la Fournaise volcano: 1. Location of tremor sources. J Volcanol Geotherm Res 147(3–4):268–290. https://doi.org/10.1016/j.jvolgeores.2005.04.005

Beroza GC, Ide S (2011) Slow earthquakes and nonvolcanic tremor. Annu Rev Earth Planet Sci 39(1):271–296. https://doi.org/10.1146/annurev-earth-040809-152531

Bird P (2003) An updated digital model of plate boundaries. Geochem Geophys Geosyst. https://doi.org/10.1029/2001GC000252

Doi I, Maeda T (2020) Landslide characteristics revealed by high-frequency seismic waves from the 2017 landslide in central Japan. Seismol Res Lett 91(5):2719–2729. https://doi.org/10.1785/0220200032

Ekström G, Nettles M, Dziewoński A (2012) The global CMT project 2004–2010: centroid-moment tensors for 13,017 earthquakes. Phys Earth Planet Inter 200–201:1–9. https://doi.org/10.1016/j.pepi.2012.04.002

Hirose H, Obara K (2005) Repeating short- and long-term slow slip events with deep tremor activity around the Bungo channel region, southwest Japan. Earth Planets Space 57(10):961–972. https://doi.org/10.1186/BF03351875

Hirose H, Hirahara K, Kimata F, Fujii N, Miyazaki S (1999) A slow thrust slip event following the two 1996 Hyuganada Earthquakes beneath the Bungo Channel, southwest Japan. Geophys Res Lett 26(21):3237–3240. https://doi.org/10.1029/1999GL010999

Hirose I, Kawasaki I, Okada Y, Sagiya T, Tamura Y (2000) A silent earthquake of December 9, 1989, in the Tokyo Bay, as revealed by the continuous observation of crustal movements in the southern Kanto district, central Japan. Zisin (J Seismol Soc Jpn 2nd Ser) 53(1):11–23. https://doi.org/10.4294/zisin1948.53.1_11

Hirose F, Maeda K, Kamigaichi O (2019) Tidal forcing of interplate earthquakes along the Tonga-Kermadec Trench. J Geophys Res Solid Earth 124(10):10,498-10,521. https://doi.org/10.1029/2019JB018088

Houston H, Delbridge BG, Wech AG, Creager KC (2011) Rapid tremor reversals in Cascadia generated by a weakened plate interface. Nat Geosci 4(6):404–409. https://doi.org/10.1038/ngeo1157

Ichihara M, Matsumoto S (2017) Relative source locations of continuous tremor before and after the subplinian events at Shinmoe-dake, in 2011. Geophys Res Lett 44(21):10,871-10,877. https://doi.org/10.1002/2017GL075293

Ichimura M, Yokoo A, Kagiyama T, Yoshikawa S, Inoue H (2018) Temporal variation in source location of continuous tremors before ash–gas emissions in January 2014 at Aso Volcano, Japan. Earth Planets Space 70(1):125. https://doi.org/10.1186/s40623-018-0895-4

Ide S (2010) Striations, duration, migration and tidal response in deep tremor. Nature 466(7304):356–359. https://doi.org/10.1038/nature09251

Ide S, Beroza GC, Shelly DR, Uchide T (2007) A scaling law for slow earthquakes. Nature 447(7140):76–79. https://doi.org/10.1038/nature05780

Ito Y, Obara K (2006) Dynamic deformation of the accretionary prism excites very low frequency earthquakes. Geophys Res Lett 33(2):L02311. https://doi.org/10.1029/2005GL025270

Ito Y, Obara K, Shiomi K, Sekine S, Hirose H (2007) Slow earthquakes coincident with episodic tremors and slow slip events. Science 315(5811):503–506. https://doi.org/10.1126/science.1134454

Ito Y, Obara K, Matsuzawa T, Maeda T (2009) Very low frequency earthquakes related to small asperities on the plate boundary interface at the locked to aseismic transition. J Geophys Res Solid Earth. https://doi.org/10.1029/2008JB006036

Ito Y, Hino R, Kido M, Fujimoto H, Osada Y, Inazu D, Ohta Y, Iinuma T, Ohzono M, Miura S, Mishina M, Suzuki K, Tsuji T, Ashi J (2013) Episodic slow slip events in the Japan subduction zone before the 2011 Tohoku-Oki earthquake. Tectonophysics 600:14–26. https://doi.org/10.1016/j.tecto.2012.08.022

Jolly A, Thompson G, Norton G (2002) Locating pyroclastic flows on Soufriere Hills Volcano, Montserrat, West Indies, using amplitude signals from high dynamic range instruments. J Volcanol Geotherm Res 118(3–4):299–317. https://doi.org/10.1016/S0377-0273(02)00299-8

Kao H, Shan SJJ, Dragert H, Rogers G, Cassidy JF, Ramachandran K (2005) A wide depth distribution of seismic tremors along the northern Cascadia margin. Nature 436(7052):841–844. https://doi.org/10.1038/nature03903

Katakami S, Yamashita Y, Yakiwara H, Shimizu H, Ito Y, Ohta K (2017) Tidal response in shallow tectonic tremors. Geophys Res Lett 44(19):9699–9706. https://doi.org/10.1002/2017GL074060

Kato A, Nakagawa S (2020) Detection of deep low-frequency earthquakes in the Nankai subduction zone over 11 years using a matched filter technique. Earth Planets Space 72(1):128. https://doi.org/10.1186/s40623-020-01257-4

Kato A, Obara K, Igarashi T, Tsuruoka H, Nakagawa S, Hirata N (2012) Propagation of slow slip leading up to the 2011 Mw 9.0 Tohoku-Oki earthquake. Science 335(6069):705–708. https://doi.org/10.1126/science.1215141

Kumagai H, Palacios P, Maeda T, Castillo DB, Nakano M (2009) Seismic tracking of lahars using tremor signals. J Volcanol Geotherm Res 183(1–2):112–121. https://doi.org/10.1016/j.jvolgeores.2009.03.010

Kumagai H, Nakano M, Maeda T, Yepes H, Palacios P, Ruiz M, Arrais S, Vaca M, Molina I, Yamashina T (2010) Broadband seismic monitoring of active volcanoes using deterministic and stochastic approaches. J Geophys Res Solid Earth 115(8):1–21. https://doi.org/10.1029/2009JB006889

Kumagai H, Lacson R, Maeda Y, Figueroa MS, Yamashina T, Ruiz M, Palacios P, Ortiz H, Yepes H (2013) Source amplitudes of volcano-seismic signals determined by the amplitude source location method as a quantitative measure of event size. J Volcanol Geotherm Res 257:57–71. https://doi.org/10.1016/j.jvolgeores.2013.03.002

Kumagai H, Londoño JM, Maeda Y, Acevedo Rivas AE (2019) Amplitude source location method with depth-dependent scattering and attenuation structures: application at Nevado del Ruiz Volcano, Colombia. J Geophys Res Solid Earth 124(11):11,585-11,600. https://doi.org/10.1029/2019JB018156

Kurihara R, Obara K, Takeo A, Maeda T (2018) Migration of deep low-frequency tremor triggered by teleseismic earthquakes in the southwest Japan subduction zone. Geophys Res Lett 45(8):3413–3419. https://doi.org/10.1002/2017GL076779

Linde AT, Gladwin MT, Johnston MJS, Gwyther RL, Bilham RG (1996) A slow earthquake sequence on the San Andreas fault. Nature 383(6595):65–68. https://doi.org/10.1038/383065a0

Nakanishi A, Takahashi N, Park JO, Miura S, Kodaira S, Kaneda Y, Hirata N, Iwasaki T, Nakamura M (2002) Crustal structure across the coseismic rupture zone of the 1944 Tonankai earthquake, the central Nankai Trough seismogenic zone. J Geophys Res Solid Earth 107(B1):EPM2. https://doi.org/10.1029/2001JB000424

Nakano M, Yabe S, Sugioka H, Shinohara M, Ide S (2019) Event size distribution of shallow tectonic tremor in the Nankai Trough. Geophys Res Lett 46(11):5828–5836. https://doi.org/10.1029/2019GL083029

Nakata R, Suda N, Tsuruoka H (2008) Non-volcanic tremor resulting from the combined effect of Earth tides and slow slip events. Nat Geosci 1(10):676–678. https://doi.org/10.1038/ngeo288

National Research Institute for Earth Science and Disaster Resilience (2019) NIED DONET. https://doi.org/10.17598/nied.0008

Nishikawa T, Matsuzawa T, Ohta K, Uchida N, Nishimura T, Ide S (2019) The slow earthquake spectrum in the Japan Trench illuminated by the S-net seafloor observatories. Science 365(6455):808–813. https://doi.org/10.1126/science.aax5618

NOAA National Centers for Environmental Information (2009) ETOPO1 global relief model. https://doi.org/10.7289/V5C8276M

Noda A, Saito T, Fukuyama E (2018) Slip-deficit rate distribution along the Nankai Trough, southwest Japan, with elastic lithosphere and viscoelastic asthenosphere. J Geophys Res Solid Earth 123(9):8125–8142. https://doi.org/10.1029/2018JB015515

Obana K, Kodaira S (2009) Low-frequency tremors associated with reverse faults in a shallow accretionary prism. Earth Planet Sci Lett 287(1–2):168–174. https://doi.org/10.1016/j.epsl.2009.08.005

Obara K (2002) Nonvolcanic deep tremor associated with subduction in southwest Japan. Science 296(5573):1679–1681. https://doi.org/10.1126/science.1070378

Obara K, Ito Y (2005) Very low frequency earthquakes excited by the 2004 off the Kii peninsula earthquakes: a dynamic deformation process in the large accretionary prism. Earth Planets Space 57(4):321–326. https://doi.org/10.1186/BF03352570

Obara K, Kato A (2016) Connecting slow earthquakes to huge earthquakes. Science 353(6296):253–257. https://doi.org/10.1126/science.aaf1512

Obara K, Hirose H, Yamamizu F, Kasahara K (2004) Episodic slow slip events accompanied by non-volcanic tremors in southwest Japan subduction zone. Geophys Res Lett 31(23):L23,602. https://doi.org/10.1029/2004GL020848

Ogiso M, Yomogida K (2012) Migration of tremor locations before the 2008 eruption of Meakandake Volcano, Hokkaido, Japan. J Volcanol Geotherm Res 217–218:8–20. https://doi.org/10.1016/j.jvolgeores.2011.12.005

Ogiso M, Yomogida K (2015) Estimation of locations and migration of debris flows on Izu-Oshima Island, Japan, on 16 October 2013 by the distribution of high frequency seismic amplitudes. J Volcanol Geotherm Res 298:15–26. https://doi.org/10.1016/j.jvolgeores.2015.03.015

Okada Y, Kasahara K, Hori S, Obara K, Sekiguchi S, Fujiwara H, Yamamoto A (2004) Recent progress of seismic observation networks in Japan—Hi-net, F-net, K-NET and KiK-net—. Earth Planets Space. https://doi.org/10.1186/BF03353076

Park JO, Naruse H, Bangs NL (2014) Along-strike variations in the Nankai shallow décollement properties and their implications for tsunami earthquake generation. Geophys Res Lett 41(20):7057–7064. https://doi.org/10.1002/2014GL061096

Pérez-Guillén C, Tsunematsu K, Nishimura K, Issler D (2019) Seismic location and tracking of snow avalanches and slush flows on Mt. Fuji Japan. Earth Surf Dyn 7(4):989–1007. https://doi.org/10.5194/esurf-7-989-2019

Plata-Martinez R, Ide S, Shinohara M, Garcia ES, Mizuno N, Dominguez LA, Taira T, Yamashita Y, Toh A, Yamada T, Real J, Husker A, Cruz-Atienza VM, Ito Y (2021) Shallow slow earthquakes to decipher future catastrophic earthquakes in the Guerrero seismic gap. Nat Commun 12(1):3976. https://doi.org/10.1038/s41467-021-24210-9

Rogers G, Dragert H (2003) Episodic tremor and slip on the Cascadia subduction zone: the chatter of silent slip. Science 300(5627):1942–1943. https://doi.org/10.1126/science.1084783

Sagae K, Nakahara H, Nishimura T, Imanishi K (2021) High resolution location of deep low-frequency tremors beneath the Kii Peninsula, Nankai subduction zone, Japan, using data from a dense seismic array. Geophys J Int 225(2):775–788. https://doi.org/10.1093/gji/ggab004

Sagiya T (2004) A decade of GEONET: 1994–2003—the continuous GPS observation in Japan and its impact on earthquake studies. Earth Planets Space. https://doi.org/10.1186/BF03353077

Shelly DR, Beroza GC, Ide S (2007) Non-volcanic tremor and low-frequency earthquake swarms. Nature 446(7133):305–307. https://doi.org/10.1038/nature05666

Sit S, Brudzinski M, Kao H (2012) Detecting tectonic tremor through frequency scanning at a single station: application to the Cascadia margin. Earth Planet Sci Lett 353–354:134–144. https://doi.org/10.1016/j.epsl.2012.08.002

Sugioka H, Okamoto T, Nakamura T, Ishihara Y, Ito A, Obana K, Kinoshita M, Nakahigashi K, Shinohara M, Fukao Y (2012) Tsunamigenic potential of the shallow subduction plate boundary inferred from slow seismic slip. Nat Geosci 5(6):414–418. https://doi.org/10.1038/ngeo1466

Takemura S, Matsuzawa T, Noda A, Tonegawa T, Asano Y, Kimura T, Shiomi K (2019a) Structural characteristics of the Nankai Trough shallow plate boundary inferred from shallow very low frequency earthquakes. Geophys Res Lett 46(8):4192–4201. https://doi.org/10.1029/2019GL082448

Takemura S, Noda A, Kubota T, Asano Y, Matsuzawa T, Shiomi K (2019b) Migrations and clusters of shallow very low frequency earthquakes in the regions surrounding shear stress accumulation peaks along the Nankai Trough. Geophys Res Lett 46(21):11,830-11,840. https://doi.org/10.1029/2019GL084666

Takemura S, Yabe S, Emoto K (2020) Modelling high-frequency seismograms at ocean bottom seismometers: effects of heterogeneous structures on source parameter estimation for small offshore earthquakes and shallow low-frequency tremors. Geophys J Int 223(3):1708–1723. https://doi.org/10.1093/gji/ggaa404

Takeo A, Idehara K, Iritani R, Tonegawa T, Nagaoka Y, Nishida K, Kawakatsu H, Tanaka S, Miyakawa K, Iidaka T, Obayashi M, Tsuruoka H, Shiomi K, Obara K (2010) Very broadband analysis of a swarm of very low frequency earthquakes and tremors beneath Kii Peninsula, SW Japan. Geophys Res Lett 37(L06):311. https://doi.org/10.1029/2010GL042586

Tamaribuchi K, Kobayashi A, Nishimiya T, Hirose F, Annoura S (2019) Characteristics of shallow low-frequency earthquakes off the Kii Peninsula, Japan, in 2004 revealed by ocean bottom seismometers. Geophys Res Lett 46(23):13,737-13,745. https://doi.org/10.1029/2019GL085158

Tanaka S, Matsuzawa T, Asano Y (2019) Shallow low-frequency tremor in the northern Japan Trench subduction zone. Geophys Res Lett 46(10):5217–5224. https://doi.org/10.1029/2019GL082817

To A, Obana K, Sugioka H, Araki E, Takahashi N, Fukao Y (2015) Small size very low frequency earthquakes in the Nankai accretionary prism, following the 2011 Tohoku-Oki earthquake. Phys Earth Planet Inter 245:40–51. https://doi.org/10.1016/j.pepi.2015.04.007

Toh A, Obana K, Araki E (2018) Distribution of very low frequency earthquakes in the Nankai accretionary prism influenced by a subducting-ridge. Earth Planet Sci Lett 482:342–356. https://doi.org/10.1016/j.epsl.2017.10.062

Wallace LM, Webb SC, Ito Y, Mochizuki K, Hino R, Henrys S, Schwartz SY, Sheehan AF (2016) Slow slip near the trench at the Hikurangi subduction zone, New Zealand. Science 352(6286):701–704. https://doi.org/10.1126/science.aaf2349

Walsh B, Jolly AD, Procter J (2017) Calibrating the amplitude source location (ASL) method by using active seismic sources: an example from Te Maari volcano, Tongariro National Park, New Zealand. Geophys Res Lett 44(8):3591–3599. https://doi.org/10.1002/2017GL073000

Walsh B, Procter J, Lokmer I, Thun J, Hurst T, Christenson B, Jolly A (2019) Geophysical examination of the 27 April 2016 Whakaari/White Island, New Zealand, eruption and its implications for vent physiognomies and eruptive dynamics. Earth Planets Space 71(1):25. https://doi.org/10.1186/s40623-019-1003-0

Wessel P, Smith WHF, Scharroo R, Luis J, Wobbe F (2013) Generic mapping tools: improved version released. Eos Trans Am Geophys Union 94(45):409–410. https://doi.org/10.1002/2013EO450001

Yabe S, Tonegawa T, Nakano M (2019) Scaled energy estimation for shallow slow earthquakes. J Geophys Res Solid Earth 124(2):1507–1519. https://doi.org/10.1029/2018JB016815

Yabe S, Baba S, Tonegawa T, Nakano M, Takemura S (2021) Seismic energy radiation and along-strike heterogeneities of shallow tectonic tremors at the Nankai Trough and Japan Trench. Tectonophysics 800(228):714. https://doi.org/10.1016/j.tecto.2020.228714

Yamamoto Y, Ariyoshi K, Yada S, Nakano M, Hori T (2022) Spatio-temporal distribution of shallow very-low-frequency earthquakes between December 2020 and January 2021 in Kumano-nada, Nankai subduction zone, detected by a permanent seafloor seismic network. Earth Planets Space 74(1):14. https://doi.org/10.1186/s40623-022-01573-x

Yamasato H (1997) Quantitative analysis of pyroclastic flows using infrasonic and seismic data at Unzen Volcano, Japan. J Phys Earth 45(6):397–416. https://doi.org/10.4294/jpe1952.45.397

Yamashita Y, Yakiwara H, Asano Y, Shimizu H, Uchida K, Hirano S, Umakoshi K, Miyamachi H, Nakamoto M, Fukui M, Kamizono M, Kanehara H, Yamada T, Shinohara M, Obara K (2015) Migrating tremor off southern Kyushu as evidence for slow slip of a shallow subduction interface. Science 348(6235):676–679. https://doi.org/10.1126/science.aaa4242

Yamashita Y, Shinohara M, Yamada T (2021) Shallow tectonic tremor activities in Hyuga-nada, Nankai subduction zone, based on long-term broadband ocean bottom seismic observations. Earth Planets Space 73(1):196. https://doi.org/10.1186/s40623-021-01533-x

Publisher's Note